

GAUSSIAN RANDOM FIELD POWER SPECTRUM AND THE SÉRSIC LAW

CARLO NIPOTI

Department of Physics and Astronomy, Bologna University, viale Berti-Pichat 6/2, 40127 Bologna, Italy

Accepted 2015 May 4

ABSTRACT

The surface-brightness profiles of galaxies are well described by the Sérsic law: systems with high Sérsic index m have steep central profiles and shallow outer profiles, while systems with low m have shallow central profiles and steep outer profiles. R. Cen (2014, ApJL, 790, L24) has conjectured that these profiles arise naturally in the standard cosmological model with initial density fluctuations represented by a Gaussian random field (GRF). We explore and confirm this hypothesis with N -body simulations of dissipationless collapses in which the initial conditions are generated from GRFs with different power spectra. The numerical results show that GRFs with more power on small scales lead to systems with higher m . In our purely dissipationless simulations the Sérsic index is in the range $2 \lesssim m \lesssim 6.5$. It follows that systems with Sérsic index as low as $m \approx 2$ can be produced by coherent dissipationless collapse, while high- m systems can be obtained if the assembly history is characterized by several mergers. As expected, dissipative processes appear to be required to obtain exponential profiles ($m \approx 1$).

Subject headings: galaxies: bulges — galaxies: elliptical and lenticular, cD — galaxies: formation — galaxies: fundamental parameters — galaxies: structure

1. INTRODUCTION

The surface-brightness profiles of spheroidal and disk components of galaxies are well described by the Sérsic (1968) law

$$I(R) = I_e \exp \left\{ -b(m) \left[\left(\frac{R}{R_e} \right)^{1/m} - 1 \right] \right\}, \quad (1)$$

where R_e is the effective radius, m is the Sérsic index, $I_e \equiv I(R_e)$ is the surface brightness at the effective radius and $b(m) \simeq 2m - 1/3 + 4/(405m)$ (Ciotti & Bertin 1999). When m is high the central profile is steep and the outer profile is shallow, while when m is low the central profile is shallow and the outer profile is steep. Recently Cen (2014) has envisaged that these profiles arise naturally in the standard cosmological model with initial density fluctuations represented by a Gaussian random field (GRF). The underlying idea is that central concentrations of stars and extended envelopes are formed by the late infall and accretion of substructures. Therefore, if the fluctuation field is dominated by long-wavelength modes the formation of the galaxy, due to the absence of significant substructures, is mainly determined by a coherent collapse, and the final profile will be shallow in the center and steep in the outskirts (an extreme case is the exponential profile $m = 1$, which is typical for disks). If the fluctuation field is dominated by short-wavelength modes there is substantial late infall of substructures and the final profile will be steeply rising toward the center and gently declining in the outskirts (as observed, for instance, in massive elliptical galaxies with $m \gtrsim 4$).

In this Letter we explore quantitatively Cen's proposal with numerical experiments in which we follow the dissipationless collapse of cold distributions of particles whose initial conditions are determined by GRFs with different power spectra. Numerical simulations of

dissipationless collapse have been run by several authors (van Albada 1982; Udry 1993; Boily et al. 2002; Nipoti et al. 2006; Joyce et al. 2009; Sylos-Labini 2013; Benhaïem & Sylos Labini 2015; Worrakitpoonpon 2015). A general finding is that the end-products have surface-density profiles well fitted by the Sérsic law (equation 1). Remarkably, this result is not specific to Newtonian gravity, as it is also found in studies of dissipationless collapses in modified gravity theories (Nipoti et al. 2007; Di Cintio et al. 2013). In Newtonian gravity the final Sérsic index is typically close to $m = 4$ (van Albada 1982; Aguilar & Merritt 1990, hereafter AM90), the value corresponding to the de Vaucouleurs (1948) profile. Though there are some indications that the final value of m can depend on the initial conditions (Trenti et al. 2005; Nipoti et al. 2006), so far there is no clear evidence of a dependence of m on the properties of the initial fluctuations. Since the seminal work of van Albada (1982) it was realized that the clumpiness of the initial conditions is an important factor in determining the nature of the collapse end-product. Clumpy initial conditions were considered in several investigations (May & van Albada 1984; McGlynn 1984; Londrillo et al. 1991; Roy & Perez 2004; Trenti et al. 2005), but in these works the inhomogeneities of the initial phase-space distribution were not systematically classified in terms of fluctuation power spectrum. An exception is Katz (1991, hereafter K91), who set up the initial conditions self-consistently from a GRF and explored different power spectra (see also Dubinski & Carlberg 1991 and Binney & Tremaine 2008, section 4.10.3).

Here we present high-resolution N -body simulations aimed at isolating the effect of the spectrum of the inhomogeneities of the initial conditions on the final density profiles of cold dissipationless collapses. We present evidence that the Sérsic index of the collapse end-product correlates with the slope of the fluctuation power spectrum of the initial conditions.

TABLE 1

PROPERTIES OF THE SIMULATIONS. P_0 AND n : AMPLITUDE AND POWER-LAW INDEX OF THE FLUCTUATION POWER-SPECTRUM OF THE INITIAL CONDITIONS. c/a AND b/a : FINAL SHORTEST-TO-LONGEST AND INTERMEDIATE-TO-LONGEST AXIS RATIOS. r_{half}/r_0 : FINAL HALF-MASS RADIUS IN UNITS OF THE SCALE RADIUS r_0 . m AND σ_m : BEST-FITTING SÉRSIC INDEX OF THE FINAL DENSITY PROFILE AND ASSOCIATED UNCERTAINTY.

Name	P_0	n	c/a	b/a	r_{half}/r_0	m	σ_m
P0	0	—	0.43	0.56	0.92	2.01	0.04
P03n3	0.3	-3	0.46	0.71	1.05	2.26	0.02
P03n25	0.3	-2.5	0.46	0.76	1.04	2.23	0.02
P03n2	0.3	-2	0.48	0.83	1.08	2.38	0.02
P03n15	0.3	-1.5	0.53	0.91	1.05	2.61	0.04
P03n1	0.3	-1	0.61	0.98	1.01	3.32	0.12
P03n05	0.3	-0.5	0.60	0.93	0.68	4.90	0.15
P03n0	0.3	0	0.63	0.92	0.50	6.43	0.11

2. NUMERICAL EXPERIMENTS

2.1. Initial conditions

The initial conditions of each simulation are built as follows. Working in Cartesian coordinates, we take a cube of edge $l_0 = 2r_0$ centered in the origin, in which we generate a GRF

$$\delta(\mathbf{x}) = \frac{1}{V} \sum_{\mathbf{k}} \delta_{\mathbf{k}} e^{i\mathbf{k} \cdot \mathbf{x}} + \delta_{-\mathbf{k}} e^{-i\mathbf{k} \cdot \mathbf{x}}, \quad (2)$$

where $\delta_{\mathbf{k}}$ and $\delta_{-\mathbf{k}}$ are independent random variables with $\delta_{-\mathbf{k}} = \delta_{\mathbf{k}}^*$, $V = l_0^3$ and the sum is performed over half of the \mathbf{k} -space (see Binney & Tremaine 2008, section 9.1.1). The GRF $\delta(\mathbf{x})$ is fully characterized by its power spectrum $P(\mathbf{k}) = \langle |\delta_{\mathbf{k}}|^2 \rangle / V$, which we parameterize as

$$P(\mathbf{k}) = \begin{cases} P_0 (k/k_0)^n & \text{if } k_0 \leq k \leq k_{\text{cutoff}} \\ 0 & \text{if } k < k_0 \text{ or } k > k_{\text{cutoff}}. \end{cases} \quad (3)$$

Here P_0 and n are, respectively, the power-spectrum amplitude and index, $k_0 = 2\pi/r_0$ is the minimum wavenumber and k_{cutoff} is the cut-off wavenumber.

We build a lattice of $N_x \times N_y \times N_z$ points equally spaced in x , y and z . At each lattice point we compute the density field¹ $\rho(x, y, z) = \rho_{\text{bg}} \exp(\delta)$, where $\rho_{\text{bg}}(r) = \rho_0 (r/r_0)^{-\gamma}$ is an unperturbed background power-law distribution ($r = \sqrt{x^2 + y^2 + z^2}$) and $\delta(x, y, z)$ is the GRF defined above. Finally, ρ is normalized to its maximum value, so $0 < \rho \leq 1$ independent of ρ_0 .

Using the standard rejection technique, we generate a spherical distribution of N equal-mass particles with $r \leq r_0$ and density distribution ρ . The x , y and z coordinates of each particle are then multiplied, respectively, by q_x , q_y and q_z to get a triaxial configuration. Velocity components v_x , v_y and v_z , extracted from a Gaussian distribution with vanishing mean and unit variance, are temporarily assigned to each particle. Once the total potential energy W and the temporary total kinetic energy T are computed, all the velocity components are multiplied by $\sqrt{\beta|W|/2T}$ in order to obtain a system with initial virial ratio β .

¹ We assume that the amplitudes of the fluctuations generated by the GRF are distributed log-normally because our initial conditions are meant to represent the non-linear phase of the collapse (Kayo et al. 2001).

2.2. Parameters of the simulations

The aim of our simulations is to isolate the effect on the end-product of dissipationless collapse of the relative contribution of short- and long-wavelength modes in the fluctuation power spectrum. Therefore, we present the results of a set of simulations differing only in the value of the power-spectrum index n , which spans the range $-3 \leq n \leq 0$ (see Table 1). In all the simulations the phases of the GRF modes are the same, as well as the other parameters determining the initial conditions: $P_0 = 0.3$, $k_{\text{cutoff}} = 6k_0$, $\gamma = 1$, $\beta = 0.01$, $q_x = 6$, $q_y = 4$, $q_z = 2$, and $N_x = N_y = N_z = 80$. For comparison, we also ran a simulation (named P0) with the same parameters as above, but no fluctuations ($P_0 = 0$).

The N -body simulations were run with the parallel collisionless code FVFPS (FORTRAN version of a fast Poisson solver; Londrillo et al. 2003; Nipoti et al. 2003), which is based on Dehnen (2002) algorithm, an efficient combination of the fast multiple method (Greengard & Rokhlin 1987) and the tree code (Barnes & Hut 1986). The main parameters of the FVFPS code are the number of particles N , the softening length ϵ , below which the Newtonian force is smoothed, and the minimum value of the opening parameter $\theta_{\text{min}} = 0.5$, which determines the mass-dependent tolerance parameter θ (analogous to the opening angle of Barnes & Hut 1986) used to control the accuracy of the force approximation (see Dehnen 2002 and Londrillo et al. 2003). In our simulations we adopted $N = 10^5$, $\theta_{\text{min}} = 0.5$ and $\epsilon = 0.02r_0$. The time-step Δt , which is the same for all particles, is allowed to vary adaptively in time as $\Delta t = 0.3/(4\pi G \rho_{\text{max}})^{1/2}$, where ρ_{max} is the maximum particle density. Each simulation runs from $t = 0$ to $t = 100t_u$, where $t_u \equiv \sqrt{r_0^3/GM}$ and M is the total mass of the N -body system. With this choice the system is fully virialized at the end of the simulation (the initial system's free-fall time is $\approx 10t_u$). The time-step values are in the range $8 \times 10^{-4} \lesssim \Delta t/t_u \lesssim 3 \times 10^{-2}$.

2.3. Results

The intrinsic and projected properties of the collapse end-products are determined as in Nipoti et al. (2006). At the end of the simulation only bound particles are selected (the mass loss is in the range 2-11%). The position of the center of the system is determined using the iterative technique described by Power et al. (2003). Following Nipoti et al. (2002), we measure the axis ratios c/a and b/a of the inertia ellipsoid of the final density distribution, its angle-averaged profile and half-mass radius r_{half} (a , b and c are, respectively, the longest, intermediate and shortest axes).

In Fig. 1 we plot the initial and final particle distributions (projected along the shortest axis), together with the final angle-averaged density profiles of four representative simulations: simulation P0 (with $P_0 = 0$) and simulations P03n3, P03n1 and P03n0 (with $P_0 = 0.3$ and, respectively, $n = -3$, $n = -1$ and $n = 0$). As apparent from the plots in the left-hand column of panels, the initial distribution becomes more and more clumpy from top (simulation P0, with homogeneous initial conditions) to bottom (simulation P03n0, in which most particles are initially in relatively few small clumps). The corresponding end-products (central column of panels of

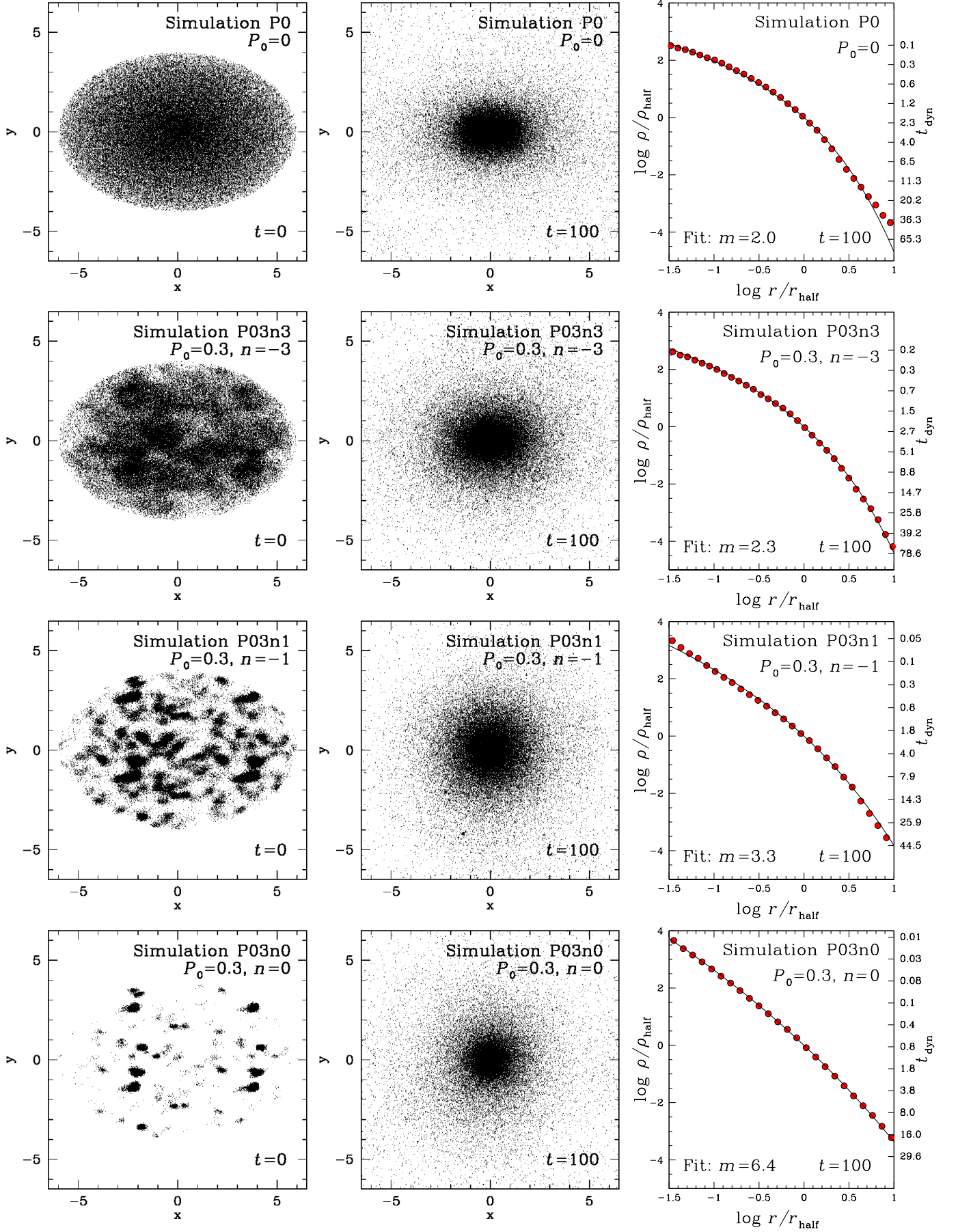


FIG. 1.— Initial (left-hand column of panels) and final (central column of panels) particle distributions (projected along the shortest axis) of simulations P0, P03n3, P03n1 and P03n0 (from top to bottom). The panels in the right-hand column show the corresponding final angle-averaged density profiles (circles) together with their best-fitting deprojected Sérsic profiles (solid curves); using the right-hand axes the circles can be interpreted as dynamical time t_{dyn} as a function of radius for the final systems. Here times are in units of t_u , x and y are in units of the scale radius r_0 , and ρ_{half} is the density at the half-mass radius r_{half} .

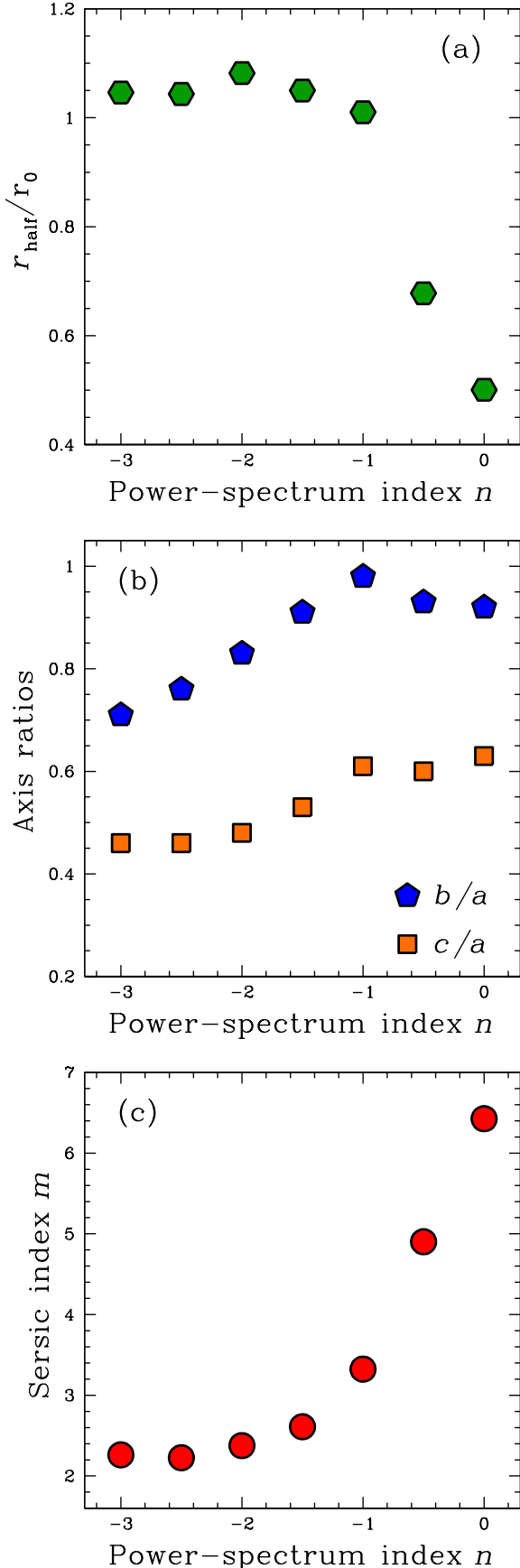


FIG. 2.— Final half-mass radius r_{half} normalized to the scale radius r_0 (panel a), axis ratios (panel b) and best-fitting Sérsic index m (panel c) as functions of the initial fluctuation power-spectrum index n of the N -body simulations P03n3, P03n25, P03n2, P03n15, P03n1, P03n05 and P03n0 (from left to right; see Table 1).

Fig. 1) tend to be more extended when the initial conditions are more homogeneous (upper plots) and more compact when the initial conditions are clumpier (lower plots). The final half-mass radius r_{half} ranges from $\approx r_0$ when $n = -3$ down to $\approx 0.5r_0$ when $n = 0$ (see Table 1 and Fig. 2a). The end-products are typically triaxial with $0.43 \lesssim c/a \lesssim 0.63$ and $0.56 \lesssim b/a \lesssim 0.98$. The trend with n is that the systems tend to be almost prolate for smooth initial conditions and almost oblate for clumpy initial conditions (see Table 1 and Fig. 2b).

The panels in the right-hand column of Fig. 1 show the final angle-averaged density profiles of the aforementioned representative simulations for $-1.5 \leq \log(r/r_{\text{half}}) \leq 1$. Over this radial range the dynamical time² $t_{\text{dyn}}(r)$ is shorter than the simulation timespan $100t_u$ (see rightmost axes in Fig. 1), so the density profiles can be considered stationary. From these plots it is apparent that, consistent with the idea of Cen (2014), the final angle-averaged density profile is steeper in the center and shallower in the outskirts when the initial conditions are clumpier. We quantify this finding by comparing the final distributions with the Sérsic law (equation 1). Under the assumption of spherical symmetry and position-independent mass-to-light ratio, the intrinsic stellar mass density distribution corresponding to equation (1) can be obtained in integral form (Ciotti 1991). A simple approximation of the deprojected Sérsic profile, which we adopt in this work, is

$$\rho(r) = \rho_{\text{half}} \left(\frac{r}{r_{\text{half}}} \right)^{-p} \exp \left[\left(\frac{r_{\text{half}}}{r_s} \right)^{\nu} - \left(\frac{r}{r_s} \right)^{\nu} \right] \quad (4)$$

(Lima Neto et al. 1999), where $\nu = 1/m$, $p = 1 - 0.6097\nu + 0.05463\nu^2$, $\rho_{\text{half}} \equiv \rho(r_{\text{half}})$ is the density at the half-mass radius and r_s is a characteristic radius related to r_{half} by

$$\ln \left(\frac{r_{\text{half}}}{r_s} \right) = \ln (1.356 - 0.0293\nu + 0.0023\nu^2) + \frac{0.6950 - \ln(\nu)}{\nu} - 0.1789. \quad (5)$$

The final angle-averaged density profiles of our N -body simulations are very well represented by the deprojected Sérsic law (equation 4). The profiles are fitted taking m as only free parameter, because r_{half} and ρ_{half} are fixed by the measured values. The fits performed over the radial range $0.04 \leq r/r_{\text{half}} \leq 10$ give values of the Sérsic index in the interval $2 \lesssim m \lesssim 6.5$ with small associated uncertainties $0.02 \lesssim \sigma_m \lesssim 0.15$ (see Table 1 and panels in the right-hand column of Fig. 1). In simulation P0 (with smooth initial conditions) we perform the fit over the smaller radial range $0.04 \leq r/r_{\text{half}} \leq 5$, because the profile has a power-law tail at large radii (see top-right panel of Fig. 1), which is reminiscent of the core-halo structure, a well-known feature of collapses starting from homogeneous initial conditions (Londrillo et al. 1991). Fig. 2c shows that the best-fitting Sérsic index m increases for increasing n : clumpier initial conditions lead to higher values of m .

² At each angle-averaged radius r we define the dynamical time as $t_{\text{dyn}}(r) = \sqrt{3\pi/16G\bar{\rho}(r)}$, where $\bar{\rho}(r) = 3M(r)/4\pi r^3$ is the average density within r and $M(r)$ is the mass contained within r .

3. DISCUSSION AND CONCLUSIONS

The results of our simulations confirm the conjecture of Cen (2014): the density profile of dissipationless collapse is steeper in the center and shallower in the outer parts if the fluctuation power spectrum of the initial conditions is dominated by short-wavelength modes. Vice versa, power spectra dominated by long-wavelength fluctuations lead to density profiles that are shallow in the center and steep in the outskirts. The end-products of our simulations have density distributions well represented by the deprojected Sérsic law with index in the range $2 \lesssim m \lesssim 6.5$. For increasing spectral index n the best-fitting Sérsic index m increases, the half-mass radius r_{half} decreases, and the systems tend to move from almost prolate to almost oblate intrinsic shape.

Of course, the exact values of the measured quantities are expected to depend on the details of the initial conditions: for instance, while here we find $m \simeq 2$ for the end-product of simulation P0 (with smooth initial $\rho \propto r^{-1}$ density profile), it is well known that the end-product of a cold collapse with smooth initial Plummer (1911) density distribution is extremely well fitted by the de Vaucouleurs (1948) $m = 4$ profile (Londrillo et al. 1991; Nipoti et al. 2006). Therefore, the above range $2 \lesssim m \lesssim 6.5$ must not be taken at face value. However, it is interesting to notice that, based on the results of the present work and of previous studies, it appears hard to get $m < 2$ with purely dissipationless processes, consistent with the expectation that the formation of $m \approx 1$ systems (typically disks) requires dissipative processes.

It is interesting to compare our results with those of previous similar investigations. A very interesting work is the paper of K91, who attempted a systematic study of the effect of GRF power spectrum on the structure of virialized systems. Though the initial conditions of K91 simulations, which were meant to represent conditions before turn-around, are different from ours in many respects, based on the results of the present work we should expect that the final density profiles of K91 depend on the initial fluctuation power spectrum. In fact, the conclusion of K91 is that the final profiles do not depend significantly on the power-spectrum slope: however, when compared to today's standard, the resolution of the simulations of K91 is rather poor (≈ 4000 particles), so it is likely that detailed differences in the density profiles were obscured by numerical noise.

A set-up in a sense more similar to ours was that of

AM90, who did not included fluctuations in their initial conditions, but considered the dissipationless collapse of smooth triaxial particle distribution with the same initial density field as our background distribution ($\rho_{\text{bg}} \propto r^{-1}$). Our simulation P0 (with no fluctuation; $P_0 = 0$) is therefore very similar to those of AM90 with virial ratio $\beta \approx 10^{-2}$ and actually, consistent AM90, we find a prolate final system with axis ratios $c/a \sim b/a \approx 1/2$. However, while we find best-fitting Sérsic index $m \simeq 2$, AM90 report that their final distributions are well fitted by $m = 4$. Again, this is likely a matter of resolution: AM90, with 5000 particles, can follow the profile down to $\approx 0.5r_{\text{half}}$, where the difference between the $m = 2$ and $m = 4$ profiles is hard to detect, while in this work we have been able to fit the profiles down to $0.04r_{\text{half}}$.

Independent support to Cen's model and to our results comes from numerical studies of dissipationless galaxy mergers. A galaxy growing in a region of the Universe dominated by fluctuations on small scales is expected to form by several mergers of smaller subunits. The finding that the best-fitting Sérsic index m increases for increasing fluctuation power-spectrum index n is therefore consistent with the results of numerical simulations showing that dissipationless mergers make the Sérsic index increase (Nipoti et al. 2003). In particular, the dissipationless accretion of small satellites is believed to be the most promising mechanism to form high- m systems (Hilz et al. 2013). However, dissipative processes can also contribute to raise m , as found for instance in simulations of mergers between gas-rich disk galaxies (e.g. Hopkins et al. 2009).

In this work we have provided quantitative support to the idea that the origin of the Sérsic law is related to the fluctuation power spectrum in the initial conditions of galaxy formation. Still, our results are based on toy models that neglect all the complexities of proper galaxy formation theories. In the future it will be interesting to explore this idea more realistically by using cosmological simulations with distinct baryonic and dark matter components, and including the all-important dissipative processes.

I am grateful to an anonymous referee for useful suggestions that helped improve this Letter. I acknowledge financial support from PRIN MIUR 2010-2011, project "The Chemical and Dynamical Evolution of the Milky Way and Local Group Galaxies", prot. 2010LY5N2T.

REFERENCES

- Aguilar, L. A., & Merritt, D. 1990, *ApJ*, 354, 33 (AM90)
 Barnes, J., & Hut, P. 1986, *Nature*, 324, 446
 Benhaiem, D., & Sylos Labini, F. 2015, *MNRAS*, 448, 2634
 Binney J., Tremaine S., 2008, *Galactic Dynamics* 2nd Ed., Princeton University Press, Princeton
 Boily, C. M., Athanassoula, E., & Kroupa, P. 2002, *MNRAS*, 332, 971
 Cen, R. 2014, *ApJ*, 790, L24
 Ciotti, L. 1991, *A&A*, 249, 99
 Ciotti, L., & Bertin, G. 1999, *A&A*, 352, 447
 Dehnen, W. 2002, *Journal of Computational Physics*, 179, 27
 de Vaucouleurs, G. 1948, *Annales d'Astrophysique*, 11, 247
 Di Cintio, P., Ciotti, L., & Nipoti, C. 2013, *MNRAS*, 431, 3177
 Dubinski, J., & Carlberg, R. G. 1991, *ApJ*, 378, 496
 Greengard, L., & Rokhlin, V. 1987, *Journal of Computational Physics*, 73, 325
 Hilz, M., Naab, T., & Ostriker, J. P. 2013, *MNRAS*, 429, 2924
 Hopkins, P. F., Hernquist, L., Cox, T. J., Keres, D., & Wuyts, S. 2009, *ApJ*, 691, 1424
 Joyce, M., Marcos, B., & Sylos Labini, F. 2009, *MNRAS*, 397, 775
 Katz, N. 1991, *ApJ*, 368, 325 (K91)
 Kayo, I., Taruya, A., & Suto, Y. 2001, *ApJ*, 561, 22
 Lima Neto, G. B., Gerbal, D., & Márquez, I. 1999, *MNRAS*, 309, 481
 Londrillo, P., Messina, A., & Stiavelli, M. 1991, *MNRAS*, 250, 54
 Londrillo, P., Nipoti, C., & Ciotti, L. 2003, *Memorie della Società Astronomica Italiana Supplementi*, 1, 18
 May, A., & van Albada, T. S. 1984, *MNRAS*, 209, 15
 McGlynn, T. A. 1984, *ApJ*, 281, 13
 Nipoti, C., Londrillo, P., & Ciotti, L. 2002, *MNRAS*, 332, 901
 Nipoti, C., Londrillo, P., & Ciotti, L. 2003, *MNRAS*, 342, 501
 Nipoti, C., Londrillo, P., & Ciotti, L. 2006, *MNRAS*, 370, 681
 Nipoti, C., Londrillo, P., & Ciotti, L. 2007, *ApJ*, 660, 256
 Plummer, H. C. 1911, *MNRAS*, 71, 460

- Power, C., Navarro, J. F., Jenkins, A., et al. 2003, MNRAS, 338, 14
- Roy, F., & Perez, J. 2004, MNRAS, 348, 62
- Sérsic, J. L. 1968, Atlas de galaxias australes. Observatorio Astronomico, Cordoba (Argentina)
- Sylos-Labini, F. 2013, MNRAS, 429, 679
- Trenti, M., Bertin, G., & van Albada, T. S. 2005, A&A, 433, 57
- Udry, S. 1993, A&A, 268, 35
- van Albada, T. S. 1982, MNRAS, 201, 939
- Worrakitpoonpon, T. 2015, MNRAS, 446, 1335